

Optical and structural properties of starch films formed on drying droplets of gelatinized starch solutions

Subhadip Ghosh and Arun Roy*

Raman Research Institute, C.V. Raman Avenue, Sadashivanagar, Bengaluru 560080, India

E-mail: aroy@rri.res.in

Abstract

We report the optical and structural properties of starch films formed on drying droplets of starch solutions on a flat substrate. The starch films formed after drying are circular in shape and have an azimuthally symmetric "M-shaped" height profile along their diameter. These films are found to be semi-crystalline in nature and transparent in visible light. Our experimental results show that these films are optically uniaxial at their center but biaxial away from the center. The variation of birefringence along the radial direction is studied for the films formed after drying droplets with different volumes and starch concentrations. The cryo-SEM studies on the drying droplets and the films reveal the micro-structures and the possible origin of birefringence of these films.

Introduction

The studies on various properties of solute films formed on drying of solution droplets casted on a flat substrate is an active field of research during last two decades. The solution

droplets of various solutes such as polymers,¹⁻³ DNA,^{4,5} nanotubes,⁶⁻⁹ nanorods,^{10,11} liquid crystals,^{12,13} colloids,¹⁴⁻¹⁷ surfactants,¹⁸ salts^{19,20} and biological materials²¹⁻²³ have been used for this purpose. The most spectacular phenomenon found after drying of such a dilute solution droplet is the coffee ring effect.^{14,15} In this phenomenon a circular stain is found to form due to the capillary flow of solute particles towards the pinned edge of the droplet. Interestingly, self-assembled structures of solute ingredients have also been found in some cases which makes the deposited thin films birefringent.^{4,8,9,12,24} It is found that the droplets with high concentration of polymer and high contact angle with the substrate produce films with distorted surface profiles after drying.^{3,25-27} In these cases, an elastic or glassy but solvent permeable skin forms on top of the droplets during drying. Further drying decreases the enclosed droplet volume which buckles the skin and produces varieties of surface distortion in the deposited films.

Starch, the most abundant and consumable carbohydrates, is the source of large polysaccharides found in nature. Starch naturally occurs in the form of grains and is made of amylose and amylopectin which are generally linear and branched polymers respectively. The starch grains on heating in excess water swell and rupture irreversibly by imbibing water above a certain temperature. This process allows the starch polysaccharides to disperse in water and is known as gelatinization of starch.²⁸ The gelatinized starch solutions casted on flat substrate produce transparent biodegradable starch films after drying.²⁹⁻³¹ In recent years, starch based bio-plastics have attracted much attention as a replacement of synthetic polymer films in plastic industries.³²

In this report, we have studied the properties of the biodegradable potato starch films formed after drying droplets of gelatinized starch solutions casted on a plastic substrate. We have investigated the drying dynamics of these droplets and find that the circular films produced after drying are linearly birefringent. The films are optically uniaxial at the center with an optic axis normal to the film whereas they are biaxial away from the center. The polarised optical microscopy studies carried out on these films establish that the three principal

axes of the indicatrix in the biaxial region of the circular films are along the radial, azimuthal and perpendicular directions respectively. We measure the variation of linear birefringence along the diameter of these films which provides valuable insight on the orientational order of starch bio-polymers developed on drying. The SEM studies on drying droplets are performed to investigate the micro-structures inside the droplets and the films. Based on these experimental results, a possible mechanism of the acquisition of optical anisotropy observed in these starch films is proposed.

Experimental

Extraction of potato starch: The starch grains were extracted from the potatoes procured locally from the market. The washed potatoes were peeled and then grated gently followed by mixing with excess water at room temperature. This mixture was stirred properly and then the dispersed starch grains in water were separated from the remnants of the grated potatoes by using a sieve. The dispersed starch grains being of slightly higher density than water precipitated after few minutes. After complete precipitation, the excess water on top of the sediment was decanted and the sedimented starch content was dried in air at room temperature for 3–4 days. The potato starch sample after complete drying appears as white powder.

Preparation of starch solutions and films: A beaker containing starch grains dispersed in water was closed tightly by using aluminum foil and kept at 90°C for 1.5 hours with continuous stirring of the sample using magnetic stirrer. At this temperature, the starch grains become completely gelatinized. The cooled sample was then homogenized using a ultrasonic probe sonicator (QSONICA Q700). The 17 ml of the starch solution was taken in a 20 ml glass vial and sonicated in pulsed mode (2 sec./4 sec. on/off) for 10 minutes with 40% amplitude of vibration using a 6 mm diameter tip. The sonicated starch solution was then cooled to room temperature by keeping it in a water bath for 5 minutes. In this

way, five different gelatinized starch solutions were prepared with concentrations 10.8 wt%, 9.5 wt%, 8.0 wt%, 6.5 wt% and 5.0 wt% respectively. Different volumes of these solutions were dropcasted on flat plastic substrates by using a micro-pipette. The droplets on complete drying at room temperature and ambient humidity produce the starch films on the substrate. The flat plastic substrates were used as the films produced can be easily detached from the substrate for further studies.

Weight measurement during drying: The weight loss during drying of a starch solution droplet was measured using a quartz crystal micro-balance with precision of 10^{-4} g. The 150 μ l of starch solution was dropcasted on the flat surface of a plastic petridish using a micro-pipette. This droplet was then allowed to dry in air at room temperature (about 25°C) and humidity in the range 53%–55%. The petridish was kept on the micro-balance and the weight readings were taken in intervals of 5 minutes till complete drying of the droplet. The weight of the droplet was calculated by subtracting the weight of the empty petridish taken prior to the dropcasting. The measurements were performed for 150 μ l droplets with different initial starch concentrations.

Polarising optical microscopy (POM) and UV-Visible spectroscopy: Both the conoscopic and orthoscopic POM studies of starch films were performed by using Olympus BX50 polarising optical microscope. The UV-Visible transmission spectroscopy studies of starch films were performed by using Lamda 35 Perkin Elmer spectrophotometer.

Measurement of linear birefringence: A He-Ne laser beam (5 mW) was passed through a polariser with its pass axis at 0° , a photo elastic modulator (PEM-100, Hinds Instruments) with its axis set at an angle of 45° to the polariser, the sample starch film and the analyser oriented at 90° to the polariser (see fig. S1 in supporting information). Then the intensity of the laser beam was monitored by using a photodiode. The radial direction of the circular starch film was set parallel to the the axis of the PEM during the measurements. The voltage

signal generated by the photo diode is

$$V = \frac{V_0}{2}[1 - \cos(\delta_R - \delta)] \quad (1)$$

where V_0 is the voltage signal corresponding to the light intensity after polariser and δ , δ_R are the linear optical phase retardations introduced by the starch film and PEM respectively. The phase retardation $\delta_R = A_0 \cos(\omega t)$, where A_0 and ω are the amplitude and frequency of sinusoidal variation of retardation in PEM. The values of these parameters were set as 2.405 radian and 50 KHz respectively.

The eqn. 1 can be expanded in Fourier series as,

$$V = V_{DC} + V_0[-J_1(A_0) \sin \delta \cos(\omega t) + J_2(A_0) \cos \delta \cos(2\omega t) + \text{higher harmonics}] \quad (2)$$

where V_{DC} is the DC part of the signal and $J_1(A_0)$, $J_2(A_0)$ are Bessel functions of first kind of order 1 and 2 respectively. The AC part of the signal was separated by a signal conditioning unit (SCU-100, Hinds Instruments) and the rms amplitudes of first (V_{1f}) and second (V_{2f}) harmonics of it were measured by a lockin amplifier (SR 830). Then from eqn. 2, the retardation of the film can be obtained as,

$$\tan \delta = \frac{J_2(A_0)}{J_1(A_0)} \times \frac{V_{1f}}{V_{2f}} \quad (3)$$

where $J_1(A_0) = J_1(2.405) = 0.5191$ and $J_2(A_0) = J_2(2.405) = 0.4317$.

The thickness profiles of the circular starch films were measured by cutting them along a diameter. The images of the cross-section of the films were taken by using a microscope (Olympus BX50) attached with a digital camera (Canon EOS 80D). These images were then analyzed by using a digital image processing software (imageJ, NIH) to obtain the thickness profiles of the films along the diameter. The linear birefringence along the diameter of a film was calculated from the ratio of the measured optical path difference and the corresponding

thickness.

Cryo-SEM studies: The droplets of volume $300 \mu\text{l}$ with 9.5 wt% starch concentration were dropcasted on a plastic petridish and left to dry in air. These droplets generally take about 18 to 20 hours to dry completely at about 25°C and 45% - 50% humidity. The liquid nitrogen was poured in the plastic petridish to freeze the droplets at different times after dropcasting to study the micro-structures. A frozen droplet was then removed from the plastic petridish and immediately fixed vertically on an aluminium sample holder by using colloidal graphene conducting paste such that half of the droplet protrudes out of the holder (see fig. S2 in supporting information). The sample with the holder was again dipped in liquid nitrogen and then transferred to the sample stage of the cryo-preparation chamber (Quorum Technologies PP3000T) kept at -170°C and the pressure maintained in this chamber was 10^{-4} to 10^{-5} mbar. The sample was then heated to -90°C and kept at this temperature for 5 minutes to make it soft for cutting through its diameter. After cutting, the newly opened cross section of the sample was left for 15 minutes at this temperature and pressure for ice sublimation followed by sputter coating it with platinum for 60 seconds. Finally, the sample was transferred to the microscope stage of the field emission scanning electron microscope (CARL ZEISS system, ULTRA PLUS model) which was kept at -190°C and the pressure maintained in the sample chamber was about 10^{-6} mbar.

X-ray diffraction (XRD) studies: A DY 1042-Empyrean (PANalytical) x-ray diffractometer with PIXcel 3D detector was used for acquiring the XRD profiles of the samples using CuK_α radiation of wavelength 1.54 \AA . The samples were kept on a flat silicon stage of the diffractometer to acquire their XRD profiles and the measurements were performed in the grazing angle of incidence of the x-ray beam. The silicon stage gives a flat XRD profile which does not interfere with sample profiles.

The XRD profiles of solution droplets during their drying were taken after dropcasting a $150 \mu\text{l}$ droplet with 9.5 wt% of initial starch concentration on a glass plate. The XRD

measurements were performed in the grazing angle of incidence of the x-ray beam. The baseline corrections were made by subtracting the profile of the empty glass plate from the sample profiles. The time interval between two successive measurements was 30 minutes.

Results and discussion

The native potato starch grains are spherical or elliptical in shape with size from about 10 μm to 60 μm . The native starch grains are semi-crystalline in nature and possess birefringent property. The potato starch grains on heating in excess water swell and ultimately disrupt on absorbing water in the temperature range from 60°C to 75°C. This irreversible transformation phenomenon is known as starch gelatinization.²⁸ In this process, starch grains lose its crystalline and birefringent property.^{33,34} The resulting gelatinized starch solution is inhomogeneous due to the presence of so called "ghost" structures of grains and the entangled starch bio-polymers.^{35,36} A homogeneous starch solution can be prepared by sonicating the gelatinized sample. Probe sonication of this sample breaks the starch bio-polymers and gives rise to a homogeneous, transparent and less viscous starch solution. These starch solutions with various initial starch concentration were dropcasted on plastic substrate and the circular transparent potato starch films were formed on drying in ambient condition.

The drying dynamics of a starch droplet on a plastic substrate was studied as a function of time after its dropcasting. Fig. 1a shows the images of a 150 μl droplet with 5 wt% starch concentration at different time intervals of its drying. Initially, the droplet dries with its edge pinned to the substrate. After about 170 minutes, the droplet edge starts to recede towards the center with the formation of a peripheral film from the initial pinned edge of the droplet. Further drying reduces the effective diameter of the central spherical cap of the sample. The time variation of the diameter of the circular edge of the droplet cap normalized by the initial diameter of the droplet is shown in fig. 1a. Initially, this normalized diameter remains constant and starts to decrease after about 170 minutes. The complete drying of this

droplet gives rise to a circular starch film with diameter same as that of the initial droplet.

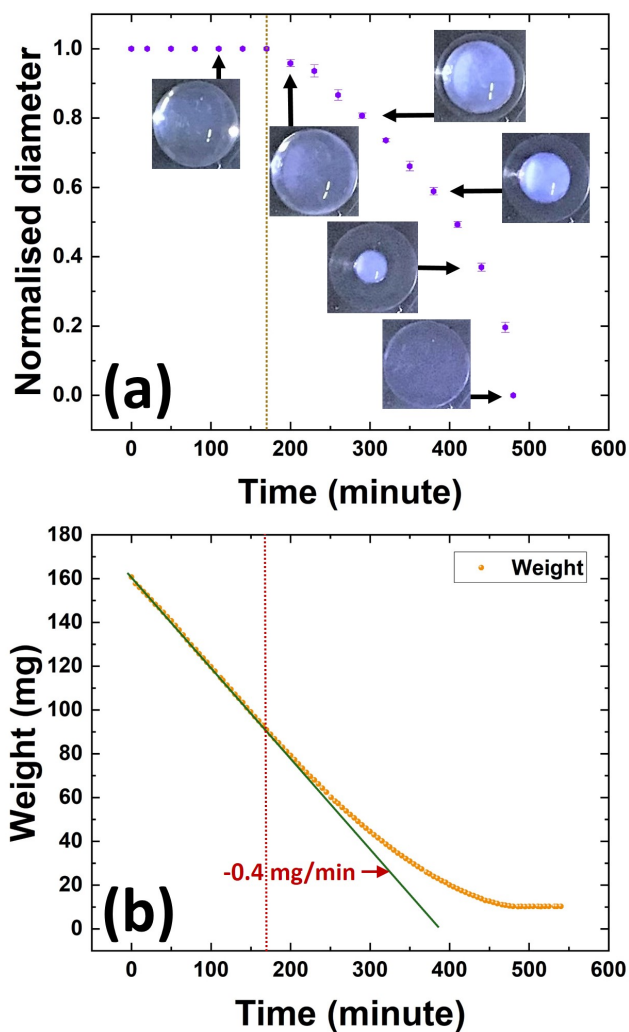


Figure 1: (a) The variation of normalized diameter of a 150 μl starch solution droplet with 5.0 wt% starch concentration during its drying. The images show the sample corresponding to some of the data points as indicated. (b) The variation of weight during its drying. The straight line (green) shows the initial linear variation of the weight.

The variation of the weight of this drying droplet with time is shown in fig. 1b. Initially, the weight of the droplet decreases linearly due to constant rate of evaporation of water which was about 0.40 mg/min. The rate of weight loss starts to decrease gradually after about 170 minutes till the complete drying of the droplet. Therefore, we find that the decrease in the rate of weight loss is correlated with the receding of the droplet edge. The sample has

negligible weight loss after its complete drying.

The similar dynamics was also found for other starch solution droplets with same initial volume but different starch concentrations. The time variation of weight for a 150 μl starch solution droplet with 9.5 wt% of initial starch concentration is shown in fig. S3 of the supporting information. Initially the weight loss rate was constant at about 0.36 mg/min and the rate started to decrease subsequently with the receding of the droplet edge which occurred above 100 minutes from its dropcasting. But our SEM studies reveal that a gel network forms in the droplet of this concentration within about 10 minutes of its dropcasting. Therefore, the decrease in the weight loss rate is independent of sol-gel transition but depends on the drying dynamics of the droplets.

The starch solution droplets after drying produce circular films on the substrate. These circular films have azimuthal symmetry with a radial variation of their thickness. Fig. 2a shows the thickness profiles along the diameter of starch films formed after drying of different volume of droplets with same initial starch concentration of 9.5 wt%. It is found that all these profiles show a sharp increase near the edge of the films and a dimple at their center giving rise to a "M-shaped" thickness profile. The films have a maximum thickness h_{max} and radius r_0 depending on the initial volume of the droplet. The normalized thickness profiles (h/h_{max}) of these films when plotted with their normalized radial distance (r/r_0), collapse to a single curve as shown in fig. 2b. Therefore, the scaled thickness profile (h/h_{max}) is a function of only the scaled radial distance (r/r_0) when other experimental parameters remain same.

Fig. 2c depicts the thickness profiles of starch films formed from the same volume of droplets (300 μl) but with different initial starch concentrations. The normalized thickness profiles (h/h_{max}) as a function of normalized radial distance (r/r_0) of the data shown in fig. 2c are plotted in fig. 2d. The dimple at the center of the film from the droplet with 10.8 wt% initial starch concentration is dipper and wider compared to that of the film formed from the droplet with 5.0 wt% initial starch concentration. Therefore, the variation of (h/h_{max})

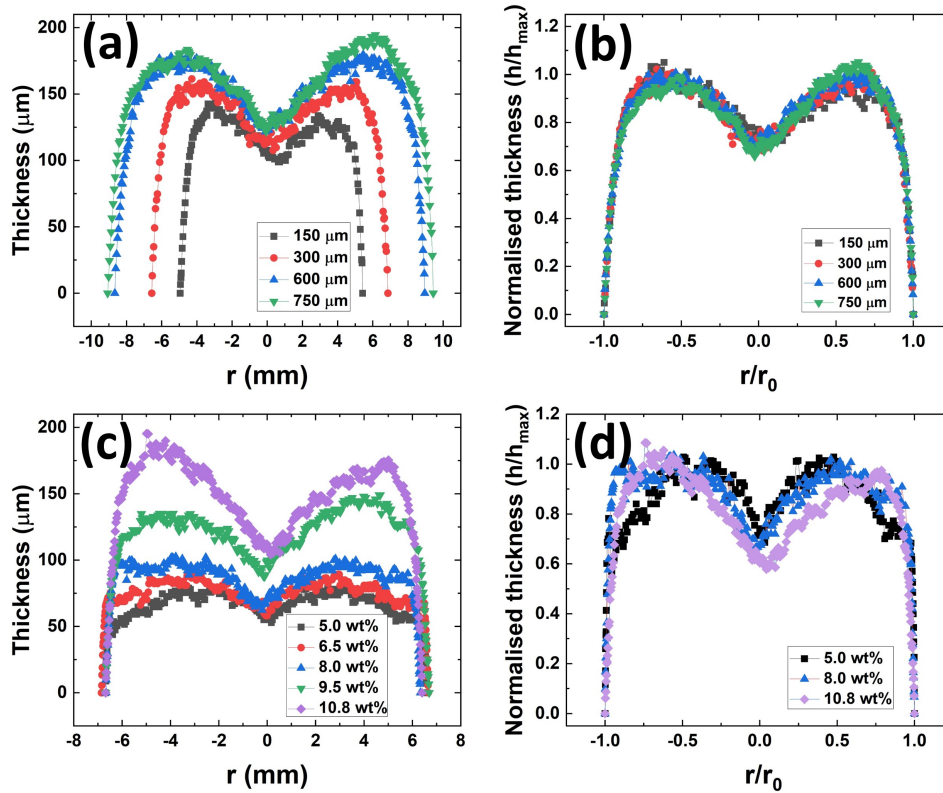


Figure 2: (a) The thickness profiles along the diameter of starch films formed from different volume of starch solution droplets with 9.5 wt% initial starch concentration. (b) The corresponding normalized thickness profiles as a function of the normalized radial distance. (c) The thickness profiles along the diameter of starch films formed from 300 μl droplets with different starch concentrations. (d) The corresponding normalized thickness profiles as a function of the normalized radial distance.

with (r/r_0) of the films depends on the initial starch concentration of the droplets.

The dried starch films are transparent in visible light. Fig. 3a shows the UV-Visible transmission spectrum of a starch film formed after complete drying of a 600 μl droplet with 9.5 wt% starch concentration. The inset of fig. 3a demonstrates the transparency of this starch film of thickness about 180 μm . The transmittance of this film is about 95% in the wavelength range from 400 nm to 1100 nm and starts to decrease below 400 nm in the UV range.

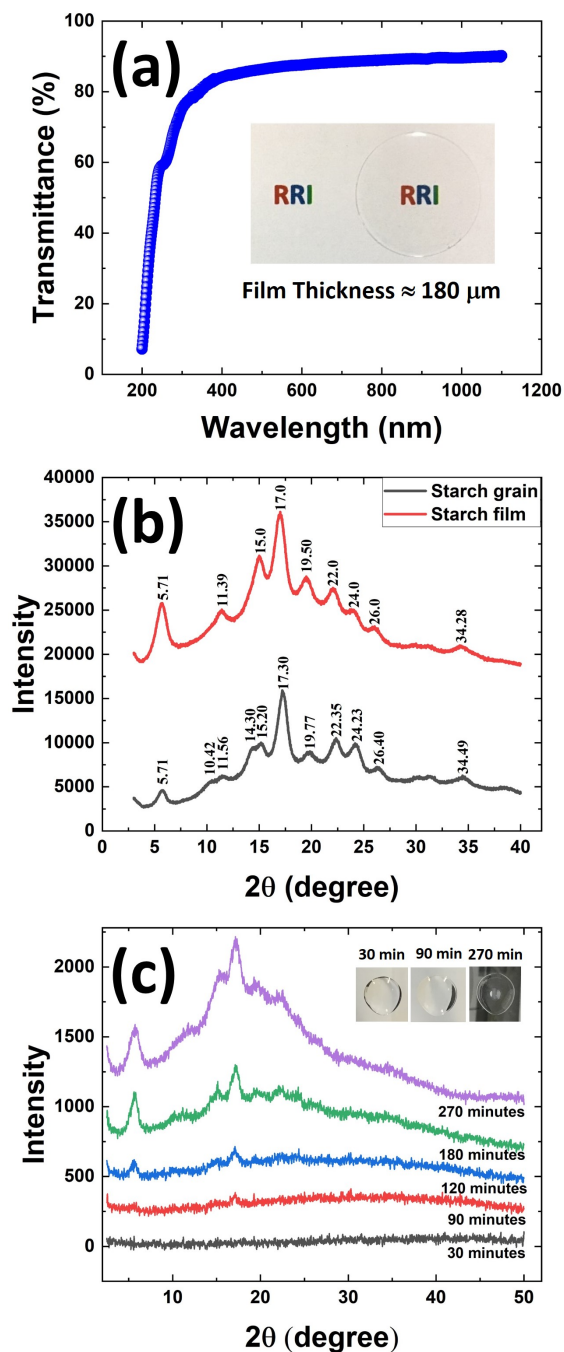


Figure 3: (a) The UV-Visible transmission spectrum of a starch film obtained on drying a droplet ($600 \mu\text{l}$, 9.5 wt%). The inset image shows the transparency of this starch film of average thickness about $180 \mu\text{m}$. (b) The XRD intensity profiles of native potato starch grains and the film. (c) The XRD profiles at different times after dropcasting a $150 \mu\text{l}$ droplet with 9.5 wt% starch concentration on a glass plate. The insets show the images of the sample at three different times during drying. The XRD intensity profiles are shifted vertically for clarity of presentation.

The XRD measurements of starch grains and starch films were performed to determine their crystalline structure. The XRD profile of potato starch grains is shown in fig. 3b. The profile exhibits peaks on top of a broad amorphous hump. This indicates that the grains are semi-crystalline in nature. The peak positions in the XRD profile of these grains are similar to that found for the potato starch grains having B-type of crystal polymorph.³⁷⁻³⁹ This type of crystal polymorph has the hexagonal lattice structure with lattice parameter $a = b = 1.85 \text{ nm}$, $c = 1.04 \text{ nm}$ and $\gamma = 120^\circ$.⁴⁰ The broad hump in this diffraction profile represents the amorphous regions of the grains coexisting with crystalline regions. The XRD profile of starch film formed from 600 μl droplet with 9.5 wt% starch concentration is also shown in fig. 3b. The diffraction peaks on a broad hump in this profile indicate that the film has semi-crystalline structure with coexistence of both crystalline and amorphous regions. The similarity of this diffraction profile to that found for the potato starch grains indicates that the film also has B-type of crystal polymorph.

The XRD studies were also carried out on a droplet during its drying on a glass plate to investigate the development of the semi-crystalline structure. The XRD profiles at different times after dropcasting a 150 μl droplet with 9.5 wt% starch concentration are shown in fig. 3c. It shows that the sample starts to acquire crystalline peaks after about 90 minutes when the droplet begins to recede from its initial edge as shown in the inset of fig. 3c. The crystalline order perhaps arises from the dried starch film starting from the peripheral region. The SEM studies show that the gel structure in droplet of this concentration forms almost immediately after its preparation. Therefore, the gel network formed initially inside the droplet does not possess crystalline order. Further drying increases the intensity of both the crystalline peaks and the broad hump till complete drying.

The circular starch films are found to be linearly birefringent. Fig. 4a shows the POM texture of a starch film formed after drying a 10 μl droplet with 10.8 wt% of starch concentration. The film between crossed polarisers appears gray-white which implies that the retardation introduced by the film is in the first order of Levy chart. The black brushes of

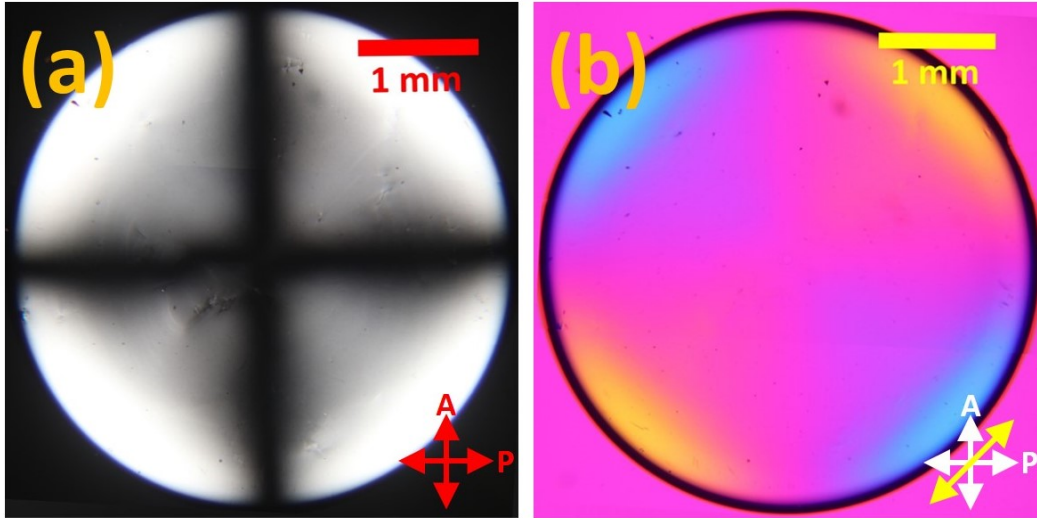


Figure 4: The POM images of the starch film (a) between crossed polarisers and (b) after inserting of a λ -plate with the slow axis at an angle of 45° with respect to the polariser.

the Maltese cross along the pass axis of polarisers divide the whole circular film into four quadrants and remain invariant on rotating the sample on the microscope stage. These observations indicate that the principal axes of index ellipse on the film are along the radial and azimuthal directions respectively. The POM studies using a λ -plate (530 nm) were performed to determine the orientation of the major axis. The introduction of the λ -plate with the slow axis at an angle of 45° with respect to the polariser changes the colour of first and third quadrants to yellow whereas second and fourth quadrants become blue as shown in fig. 4b. These colours belong to the first and second order of Levy chart respectively. Therefore the effective addition and subtraction of the optical path differences occur in the blue and yellow coloured quadrants respectively. These observations imply that the major and minor axes of the index ellipse on the sample are along the azimuthal and the radial directions of the film respectively.

The center of the film between crossed polarisers appears dark which implies that this region is either optically isotropic or uniaxial with an optic axis along the normal to the film. The conoscopic studies were performed to determine the nature of the optical anisotropy of the dried starch films. Fig. 5a shows the conoscopic figures at the center ($r = 0$) and

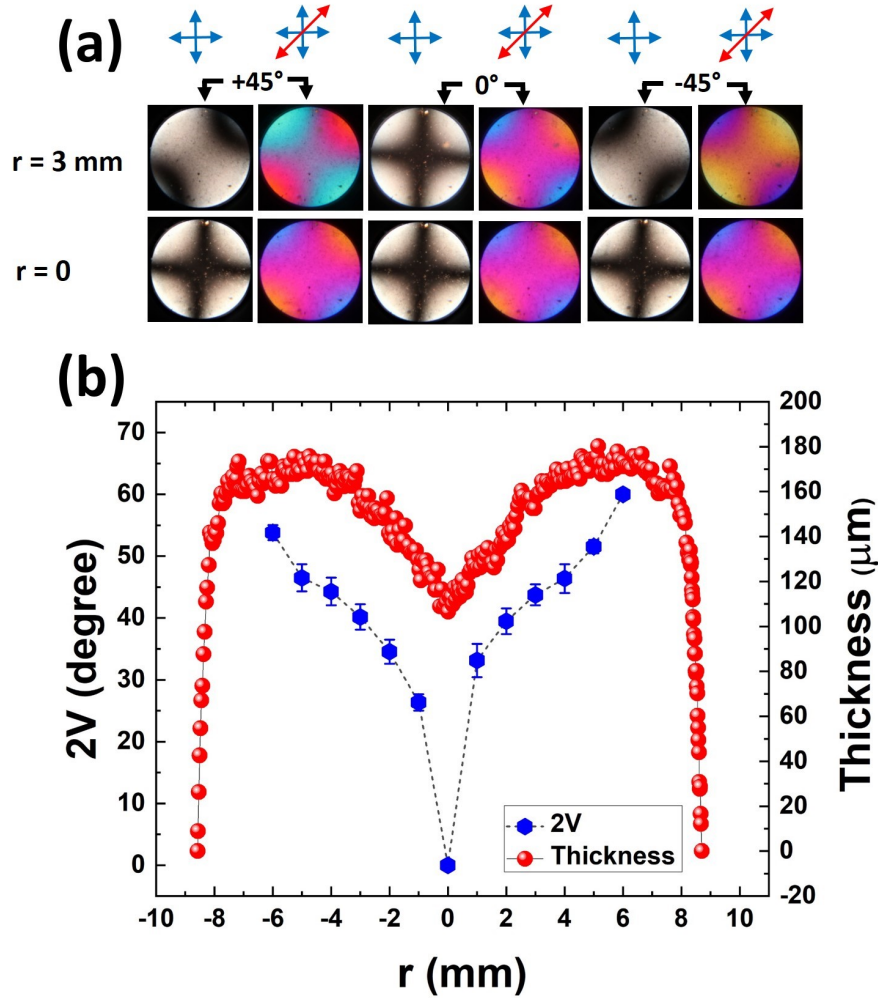


Figure 5: (a) The conoscopic figures of starch film at $r = 0$ (bottom row) and at $r = 3 \text{ mm}$ (top row) for three different orientations of the sample on microscope stage with and without the λ -plate. (b) The variation of the acute axial angle $2V$ along the radial direction of a film formed on drying of a droplet ($600 \mu\text{l}$, 9.5 wt%). The thickness profile of the film is also shown in this figure.

$r = 3 \text{ mm}$ of a starch film of diameter about 16 mm formed after drying a $600 \mu\text{l}$ droplet of concentration 9.5 wt%. The bottom row in fig. 5a shows the conoscopic figures at the center of the film for three different orientations of the sample on the microscope rotation stage in the absence and presence of a λ -plate in the optical path. The intersection point of the crossed isogyres parallel to the polarisers in the conoscopic figures without λ -plate is always at the center of the field of view. This observation confirms the optical uniaxiality of the central region with an optic axis normal to the film.⁴¹ The insertion of the λ -plate into

the optical path changed the colour of the first and third quadrants to yellow whereas the second and fourth quadrants became blue (see bottom row of fig. 5a). It can be concluded from these observations that the sign of the birefringence at the central region of the film is negative. Hence, the conoscopic studies confirm that the index ellipsoid at the center of the film has uniaxial oblate shape.

The top row in fig. 5a shows the conoscopic figures at $r = 3$ mm of the film for three different orientations of the sample on the microscope rotation stage. On rotating the film by 360° on the microscope stage, the conoscopic figures at this location show that the isogyres become crossed at four distinct positions with a difference of 90° . At $\pm 45^\circ$ with respect to a crossed position, the isogyres separate and become hyperbolic (see the top row of fig. 5a) which indicates the optical biaxiality of the film at this position.⁴¹ These hyperbolic isogyres containing the poles of the two optic axes at their apex are centered at the middle of the field of view. Further, the intersection point of the isogyres at crossed positions also lies at the center of the field of view. These observations indicate that one of the principal axis of the index ellipsoid with the refractive index denoted as α and the optic plane are perpendicular to the film at this biaxial region. The orthoscopic studies as discussed above confirm that the other principal axes with indices denoted as γ and β on the plane of film are along the azimuthal and the radial directions respectively. The conoscopic studies after inserting a λ -plate (530 nm) in the optical path were performed to determine the order of the principal indices α , β and γ at the biaxial region of the film. The insertion of the λ -plate for $+45^\circ$ orientation of the optic plane to the polariser changed the colour in the region between the uncrossed isogyres to blue whereas it became yellow at -45° orientation of the optic plane as shown in fig. 5a (top row). Therefore, from these observations it can be concluded that the film in its biaxial region is optically negative and α is the minor principal index. So the optic plane containing the major principal index γ and minor principal index α lies along the azimuthal direction and perpendicular to the film. The intermediate principal axis with the index β is along the radial direction of the film.

The film is uniaxial at its center and becomes increasingly biaxial along the radially outward direction. The acute axial angle $2V$ between the two optic axes can be measured from the conoscopic studies (see the supporting information for the detail procedure). The variation of the angle $2V$ along the diameter of a starch film formed from 600 μl solution droplet with 9.5 wt% initial starch concentration is shown in fig 5b. The angle $2V$ is zero at the uniaxial center and it increases monotonically towards the edge of the film. The hyperbolic isogyres go out of the field of view for $r > 6$ mm of the film (see fig. S6 in supporting information) and the measurement of the axial angle was not possible.

The anisotropic optical properties of these starch films arise due to the orientational order of starch bio-polymers developed during drying. Therefore, measuring the linear birefringence along the radial direction of starch films provides valuable insight on the structure of these films. Fig. 6a shows the variation of effective linear birefringence ($\gamma - \beta$) along the diameter of a starch film formed after drying a 600 μl droplet of concentration 9.5 wt% measured by using the PEM technique. This figure also shows the corresponding thickness profile of the film along its diameter. The birefringence profile along the radial direction from the center to the edge of the film can be divided into three regions with three different slopes. The measured birefringence at the center of the film is zero due to its uniaxial nature. Initially the birefringence increases rapidly along the radially outward direction from the center. Then it increases with a relatively lower slope and again increases rapidly to the maximum value near the edge of the film.

The birefringence profiles of starch films obtained on drying the same volume of droplets but with different starch concentrations were measured to investigate the effects of initial starch concentration. Fig. 6b shows the birefringence profiles of films obtained on drying 300 μl droplets with different starch concentrations. These profiles are plotted as a function of the normalized radial distance in the films. The profiles have similar characteristic variation with three different slopes along the radial direction. But the slope in the middle part of the birefringence profile decreases with decreasing the initial starch concentration. The

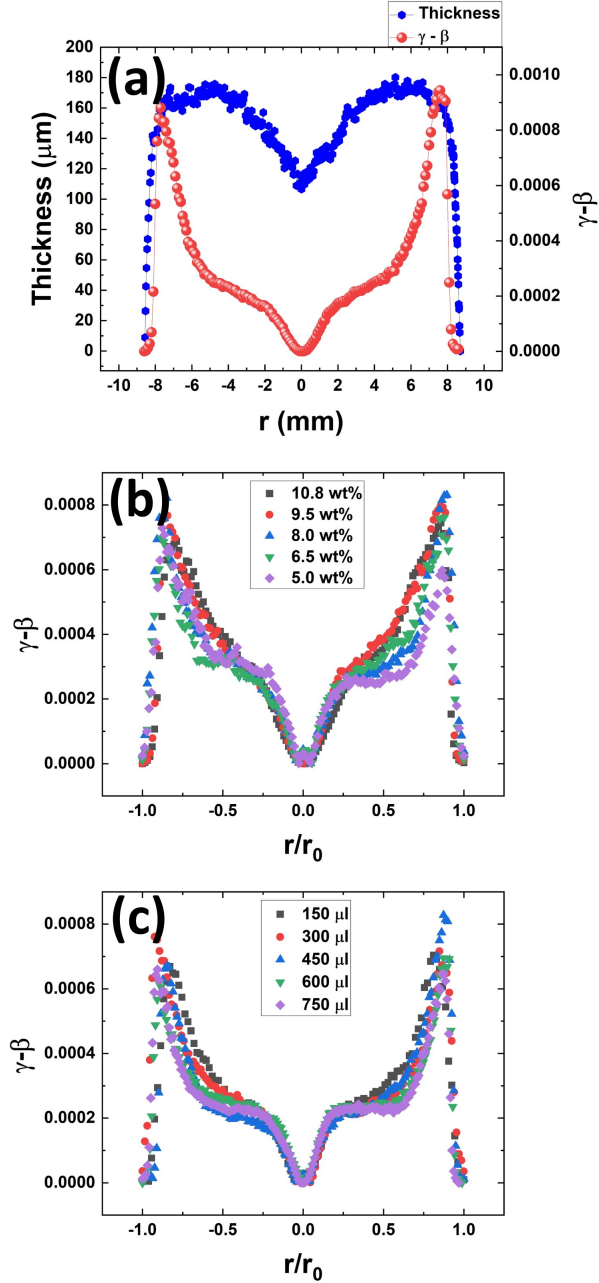


Figure 6: (a) The variation of $(\gamma - \beta)$ and thickness along the diameter of a starch film obtained from a droplet (600 μl , 9.5 wt%). The variation of $(\gamma - \beta)$ as a function of normalized radial distance on starch films formed from (b) 300 μl droplets with different starch concentrations and (c) different volumes of droplets with 6.5 wt% starch concentration.

maximum values of birefringence near the edge of these films are close to each other and hence it is independent of the initial starch concentration of droplets.

The birefringence profiles of the starch films formed after drying different volumes of

droplets but with same initial starch concentration (6.5 wt%) were measured to study the effect of initial droplet volume. These profiles as a function of the normalized radial distance (r/r_0) are shown in fig. 6c. The superposition of all these data indicates that the effective birefringence ($\gamma - \beta$) is a function of (r/r_0) only for the other experimental conditions remaining the same. The very similar values of maximum birefringence near the edge of these films implies that it does not depend on the initial volume of the droplets.

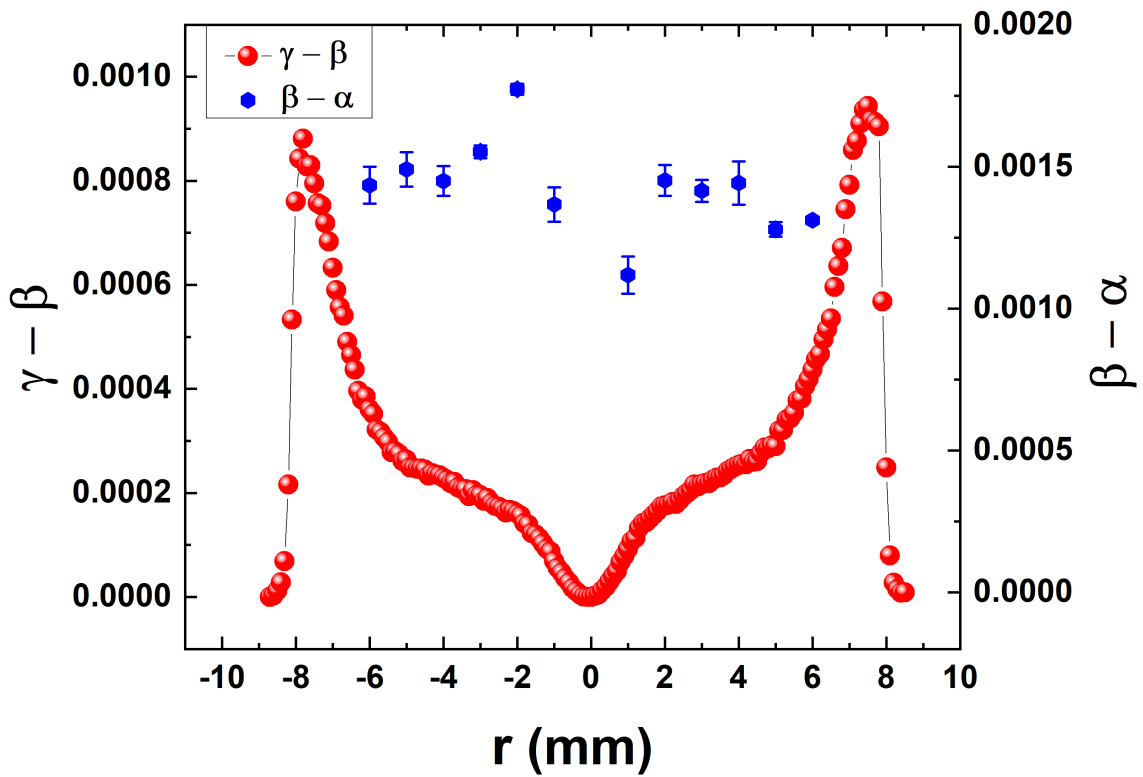


Figure 7: The variation of ($\gamma - \beta$) and ($\beta - \alpha$) along the diameter of a starch film obtained on drying of 600 μl droplet with 9.5 wt% starch concentration.

The variation of ($\beta - \alpha$) along a diameter of a starch film can be calculated from the measured values of acute axial angle $2V$ and the corresponding values of ($\gamma - \beta$) (see supporting information for more detail). Fig. 7 shows the variation of ($\beta - \alpha$) for a film obtained on drying a droplet (600 μl , 9.5 wt%) which is calculated from the measured values of $2V$ (see fig. 5b) and the values of ($\gamma - \beta$) also shown in fig. 7. It is found that although ($\gamma - \beta$) varies

considerably along the radial direction of the film but $(\beta - \alpha)$ remains almost constant.

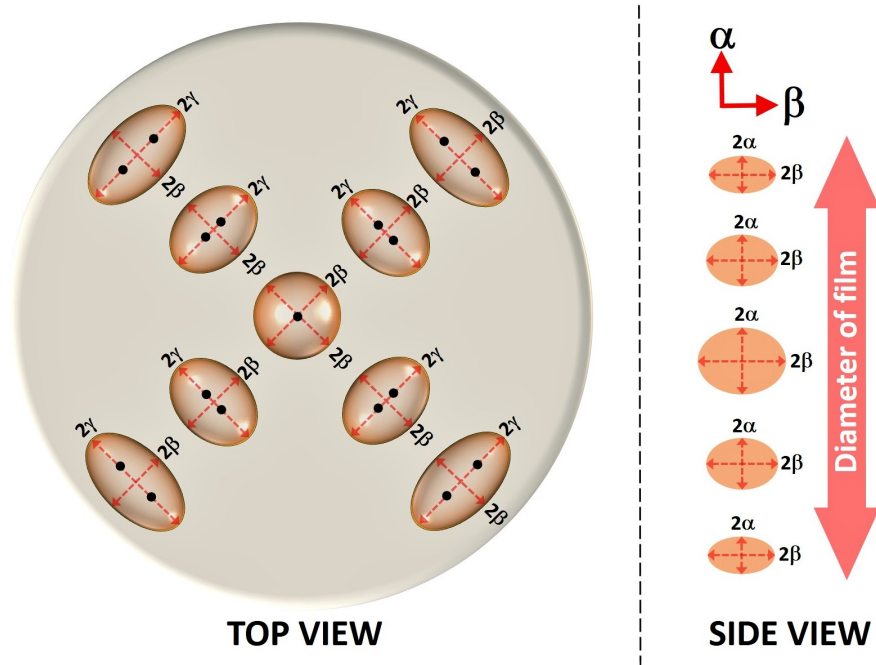


Figure 8: [Left] The schematic representation of the index ellipsoids at different positions along the diameter of a starch film. [Right] The variation of index ellipse in α - β plane along the diameter of the film.

The variation of index ellipsoid along the diameter of the starch film viewed from the top is schematically shown in the left side of fig. 8. The indicatrix in the biaxial region of the film is a general ellipsoid with three different principal indices α , β and γ along the normal, radial and azimuthal directions of the film respectively. The intersection points between the optic axes and the ellipsoid in the biaxial region are indicated by a pair of black dots on each indicatrix in this diagram. The increasing angle $2V$ between the two optic axes towards the edge of the film widens the separation between these dots along the radially outward direction. At the center of the film having uniaxial character, the index ellipsoid appears circular with the intersection point of optic axis at its center. The right hand side of fig. 8 shows the variation of index ellipse in the α - β plane along the diameter of the film. At the uniaxial center of the film, the birefringence is negative and the index ellipsoid has an oblate shape. The indices α and β have maximum values at the center of the film and they diminish

monotonically towards the edge keeping their difference almost same.

The cryo-SEM studies of drying starch droplets were carried out to investigate the sub-microscopic structures of the sample. Fig. 9a,b show the cryo-SEM textures of a vertical cross-section of a droplet (300 μl , 9.5 wt%) after 10 minutes of its dropcasting. The textures clearly show the presence of a solid thin crust of thickness about 1.3 μm on the surface of the droplet (fig. 9a) and a cellular network inside the droplet (fig. 9b). The solid crust perhaps forms due to the increase of polymer concentration near the free interface of the droplet during its drying.^{25–27,42} The cellular network observed inside the droplet can account for the gelling property of the sample. The walls of the cellular structures are composed of starch bio-polymers and starch nano-particles are found to float inside these cells (see fig. S8 in the supporting information). Similar gel network structure has also been observed during retrogradation of gelatinized starch samples.^{43,44}

The circular edge of the droplets (300 μl , 9.5 wt%) beyond about 7–8 hours starts to recede from the initial pinned edge towards the center with the formation of a peripheral film. Fig. 9c shows the SEM texture of vertical cross section of such a droplet after 14 hours of dropcasting near the receded contact line. The regions marked 1 and 2 in this figure correspond to the dried film outside and the gel just inside the droplet edge respectively. The magnified view of region 1 as shown in fig. 9d is depicting the smooth texture of the film. A mesh network structure made of filaments of starch bio-polymers is observed in the magnified view of region 2 as shown in fig. 9e. This mesh network of starch filaments ultimately gives rise to the smooth textured film after complete drying.

Fig. 9f shows the cross sectional SEM texture near the free interface of this droplet at its central region. Three different regions with different textures can be observed in this figure. The magnified view of the marked region 3 near the interface is shown in fig. 9g. The image shows the smooth texture of a dense crust which is same as that found for the dried peripheral film shown in fig. 9d. Below the crust, a mesh network region is developed by the filaments of starch bio-polymers. The width of this region is large compared to that of the crust and

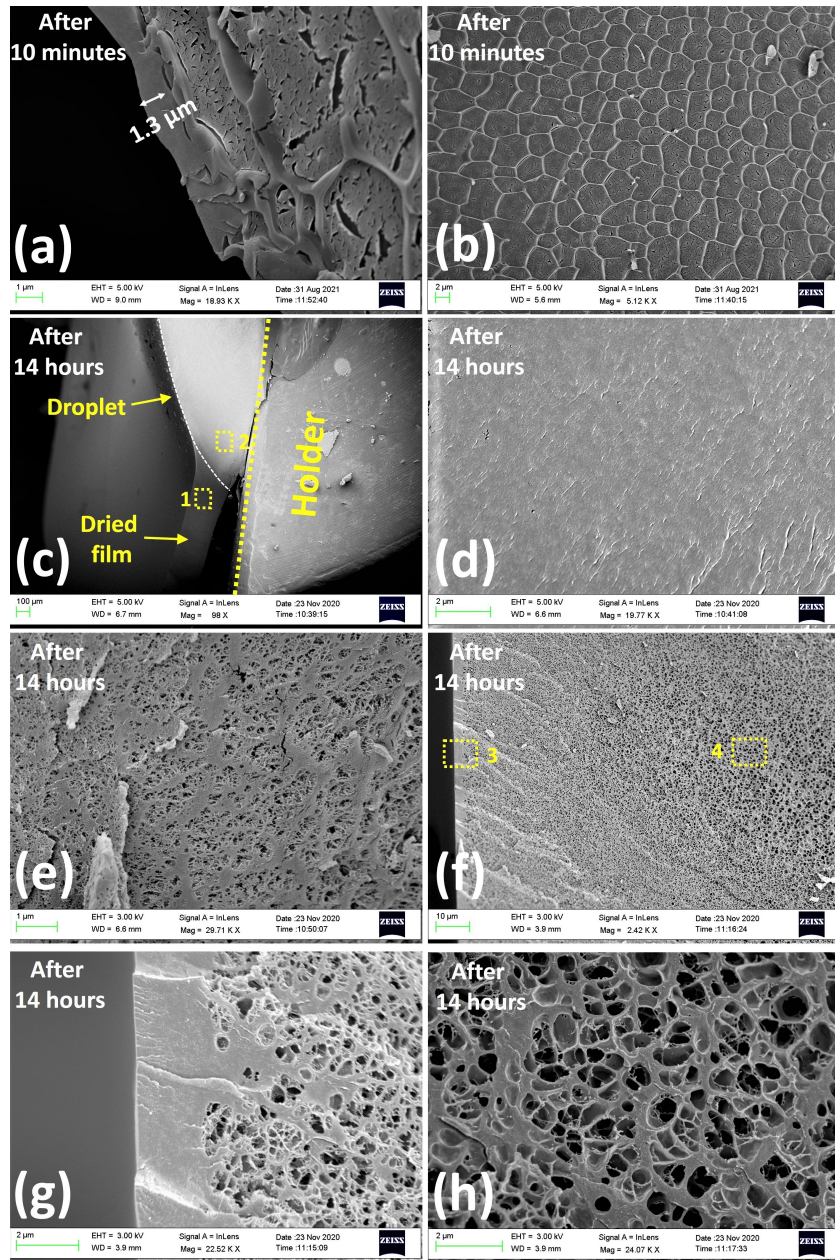


Figure 9: The cryo-SEM textures of the vertical cross section of droplets ($300 \mu\text{l}$, $9.5 \text{ wt}\%$) at different time after dropcasting. (a) The solid elastic crust on the surface of the droplet after 10 minutes. (b) The cellular network structure inside the droplet after 10 minutes. (c) The texture near the contact line after 14 hours showing the droplet and the peripheral dried film fixed on the SEM holder. The magnified views of the marked region 1 (d) and region 2 (e) showing the smooth texture of the dried starch film and the mesh network structure inside the droplet respectively. (f) The SEM texture near the central interfacial region of the droplet after 14 hours. The magnified views of the marked region 3 (g) and region 4 (h) showing the crust on top of the droplet and the cellular network structure well inside the droplet respectively.

has relatively lesser density than the crust. A cellular network structure with lowest density is observed below the mesh network region. The magnified view of the marked region 4 of this cellular structure is shown in fig. 9h which clearly reveals the membranes separating the cells. Therefore it can be inferred from the SEM studies that the drying droplet develops a relatively thinner solid elastic crust at the interface, an intermediate mesh network region below the crust and an inner core of cellular network structure. The schematic diagrams of the drying starch droplet and its vertical cross section are depicted in fig. 10. It is apparent that the cellular network structure gives rise to the denser mesh network structure near the droplet interface on drying which transforms to the dried film at the receding circular contact edge of the droplet on further drying.

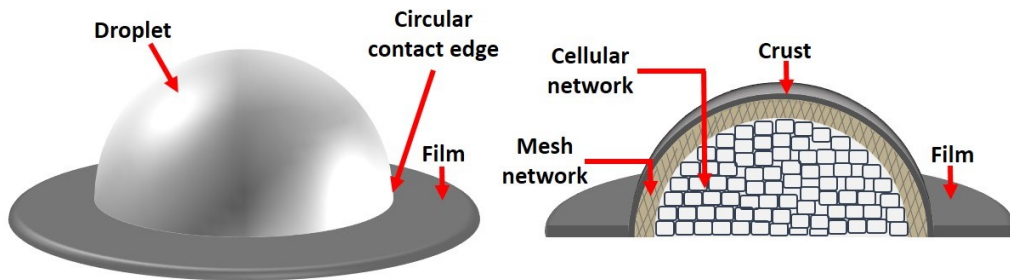


Figure 10: The schematic diagrams of the drying droplet and its vertical cross section.

It has been found that drying a droplet of dilute solution of various kind of solutes on a substrate gives rise to a circular stain which is known as coffee ring effect.^{14,15} During this drying process, the solute particles are driven by the capillary flow towards the edge of the droplet and deposited there. The dried film formed in this way shows the highest thickness near its edge. Kajiya *et al.* studied this coffee ring effect in the deposited film as a function of the concentration of a polymeric solution.³ They found that the thickness mismatch of the dried film between its rim and the center reduced with increasing the initial polymer concentration and the film became almost flat at a certain concentration. Further increase of the solute concentration again started to produce dimple at the middle of the

dried film which became dipper with increasing the solute concentration. The mechanism of this dimple formation in the films for higher solute concentration is not similar to that found in the coffee ring effect. It is proposed that this surface distortion is driven by the crust formation on the droplet interface during its drying. The similar results of surface distortion in the films formed on drying droplets of various polymer solutions were also found.²⁵⁻²⁷ In our experiments, a solid crust at the free droplet interface and a dense mesh like network structure below the crust are found to form during drying of the droplets. The dimple at the center of starch films becomes dipper and wider on increasing the initial starch concentration as shown in fig. 2. Therefore, the "M-shaped" thickness profiles of the starch films observed in our experiments perhaps can be associated with the formation of both the crust and the mesh structure near the droplet interface. The droplet with higher initial starch concentration perhaps takes relatively less time to form the crust and the mesh network near the droplet interface leading to the formation of a dipper and wider dimple in the films.

The biaxiality of the dried starch films can be explained by assuming that the starch filaments forming the mesh network structure observed experimentally are linearly birefringent. These filaments near the circular contact line of the drying droplet tend to align themselves parallel to this line. This alignment of the starch filaments perhaps gives rise to the biaxial starch film with three principal indices α , β and γ along normal, radial and azimuthal directions respectively. The alignment tendency of these filaments along the azimuthal direction gives rise to the highest index γ along this direction near the edge of the film. The other two principal directions being not equivalent during drying gives rise to the biaxiality of the film away from the center. The gradually diminishing orientational order of the filaments decreases the value of the principal index γ monotonically along the radially inward direction of the film. As a consequence of this, the value of other two principal indices α and β increases simultaneously along the same direction keeping their difference constant as found experimentally.

Conclusion

We study the drying dynamics of droplets of gelatinized potato starch solutions on a flat substrate at room temperature and humidity. The droplets are initially pinned at their circular contact line to the substrate. The droplet edge subsequently starts to recede towards the center, leaving a transparent and linearly birefringent film from its initial pinned edge. The circular starch films formed after complete drying of droplets are azimuthally symmetric and show a "M-shaped" thickness profile along their diameter. These films are partially crystalline and appear transparent in visible light. The POM studies show that the films at their center are optically uniaxial with the optic axis perpendicular to the films but biaxial away from the center. In the biaxial region, the three principal indices α , β and γ are along the normal, radial and azimuthal directions of the film respectively with $\alpha < \beta < \gamma$. Both the uniaxial and biaxial regions of the films are found to be optically negative. The effective birefringence ($\gamma - \beta$) increases along the radially outward direction of the films whereas ($\beta - \alpha$) remains almost constant. The cryo-SEM studies show that the starch solutions with time develop a cellular network structure giving rise to their gelling property. The SEM texture of the vertical cross-section of a drying droplet shows a cellular network structure at the core, an intermediate mesh region and a solid crust as the outer most layer. The intermediate mesh region consists of filaments of starch bio-polymers. The alignment of these filaments near the receding circular edge of the drying droplet perhaps gives rise to the linear birefringence of the deposited solid film.

Acknowledgement

We would like to thank Ms. Vasudha K. N. for her help in acquiring XRD data and UV-Vis transmission spectra. We also would like to thank Mr. K. M. Yatheendran for his help in cryo-SEM imaging.

Supporting Information Available

The supporting information contains (a) the schematic figure of the optical retardation measurement setup by using PEM, (b) schematic figure of a cryo-SEM holder, (c) the weight loss curve of a starch solution droplet (150 μl , 9.5 wt%) during its drying on a plastic substrate, (d) the conoscopic figures along the radial direction of a starch film formed after drying a droplet (600 μl , 9.5 wt%), (e) the cryo-SEM texture of a starch solution droplet (300 μl , 9.5 wt%) after about 10 minutes of its dropcasting and (f) the derivation of the formulas for measuring the acute axial angle $2V$ and the effective birefringence ($\beta - \alpha$).

The following files are available free of charge.

- Filename: Supporting information

References

- (1) Kajiya, T.; Kobayashi, W.; Okuzono, T.; Doi, M. Controlling the drying and film formation processes of polymer solution droplets with addition of small amount of surfactants. *The Journal of Physical Chemistry B* **2009**, *113*, 15460–15466, PMID: 19921951.
- (2) Kajiya, T.; Kaneko, D.; Doi, M. Dynamical visualization of “coffee stain phenomenon” in droplets of polymer solution via fluorescent microscopy. *Langmuir* **2008**, *24*, 12369–12374, PMID: 18844390.
- (3) Kajiya, T.; Nishitani, E.; Yamaue, T.; Doi, M. Piling-to-buckling transition in the drying process of polymer solution drop on substrate having a large contact angle. *Phys. Rev. E* **2006**, *73*, 011601.
- (4) Smalyukh, I. I.; Zribi, O. V.; Butler, J. C.; Lavrentovich, O. D.; Wong, G. C. L. Structure and dynamics of liquid crystalline pattern formation in drying droplets of DNA. *Phys. Rev. Lett.* **2006**, *96*, 177801.

- (5) Maheshwari, S.; Zhang, L.; Zhu, Y.; Chang, H.-C. Coupling between precipitation and contact-line dynamics: multiring stains and stick-slip motion. *Phys. Rev. Lett.* **2008**, *100*, 044503.
- (6) Duggal, R.; Hussain, F.; Pasquali, M. Self-assembly of single-walled carbon nanotubes into a sheet by drop drying. *Advanced Materials* **2006**, *18*, 29–34.
- (7) Zhang, S.; Li, Q.; Kinloch, I. A.; Windle, A. H. Ordering in a droplet of an aqueous suspension of single-wall carbon nanotubes on a solid substrate. *Langmuir* **2010**, *26*, 2107–2112, PMID: 19772351.
- (8) Li, Q.; Zhu, Y. T.; Kinloch, I. A.; Windle, A. H. Self-organization of carbon nanotubes in evaporating droplets. *The Journal of Physical Chemistry B* **2006**, *110*, 13926–13930, PMID: 16836343.
- (9) Zhao, Y.; Cavallaro, G.; Lvov, Y. Orientation of charged clay nanotubes in evaporating droplet meniscus. *Journal of colloid and interface science* **2015**, *440*, 68–77.
- (10) Querner, C.; Fischbein, M. D.; Heiney, P. A.; Drndić, M. Millimeter-scale assembly of CdSe nanorods into smectic superstructures by solvent drying kinetics. *Advanced Materials* **2008**, *20*, 2308–2314.
- (11) Martín, A.; Schopf, C.; Pescaglioni, A.; Wang, J. J.; Iacopino, D. Facile formation of ordered vertical arrays by droplet evaporation of Au nanorod organic solutions. *Langmuir* **2014**, *30*, 10206–10212.
- (12) Davidson, Z. S.; Huang, Y.; Gross, A.; Martinez, A.; Still, T.; Zhou, C.; Collings, P. J.; Kamien, R. D.; Yodh, A. Deposition and drying dynamics of liquid crystal droplets. *Nature communications* **2017**, *8*, 1–7.
- (13) Chu, G.; Zussman, E. From chaos to order: evaporative assembly and collective behav-

- ior in drying liquid crystal droplets. *The Journal of Physical Chemistry Letters* **2018**, *9*, 4795–4801.
- (14) Deegan, R. D.; Bakajin, O.; Dupont, T. F.; Huber, G.; Nagel, S. R.; Witten, T. A. Capillary flow as the cause of ring stains from dried liquid drops. *Nature* **1997**, *389*, 827–829.
- (15) Deegan, R. D.; Bakajin, O.; Dupont, T. F.; Huber, G.; Nagel, S. R.; Witten, T. A. Contact line deposits in an evaporating drop. *Phys. Rev. E* **2000**, *62*, 756–765.
- (16) Parisse, F.; Allain, C. Drying of colloidal suspension droplets: experimental study and profile renormalization. *Langmuir* **1997**, *13*, 3598–3602.
- (17) Haw, M.; Gillie, M.; Poon, W. Effects of phase behavior on the drying of colloidal suspensions. *Langmuir* **2002**, *18*, 1626–1633.
- (18) Shi, J.; Yang, L.; Bain, C. D. Wetting and drying of aqueous droplets containing non-ionic surfactants C_nE_m . *Langmuir* **2021**, *37*, 4091–4101, PMID: 33797926.
- (19) Basu, N.; Mukherjee, R. Evaporative drying of sodium chloride solution droplet on a thermally controlled substrate. *The Journal of Physical Chemistry B* **2020**, *124*, 1266–1274, PMID: 31990551.
- (20) Choudhury, M. D.; Dutta, T.; Tarafdar, S. Pattern formation in droplets of starch gels containing NaCl dried on different surfaces. *Colloids and Surfaces A: Physicochemical and Engineering Aspects* **2013**, *432*, 110–118.
- (21) Brutin, D.; Sobac, B.; Loquet, B.; Sampol, J. Pattern formation in drying drops of blood. *Journal of fluid mechanics* **2011**, *667*, 85–95.
- (22) Gorr, H. M.; Zueger, J. M.; McAdams, D. R.; Barnard, J. A. Salt-induced pattern formation in evaporating droplets of lysozyme solutions. *Colloids and Surfaces B: Biointerfaces* **2013**, *103*, 59–66.

- (23) Pal, A.; Gope, A.; Athair, A. S.; Iannacchione, G. S. A comparative study of the drying evolution and dried morphology of two globular proteins in de-ionized water solutions. *RSC Advances* **2020**, *10*, 16906–16916.
- (24) Beyer, S. T.; Walus, K. Controlled orientation and alignment in films of single-walled carbon nanotubes using inkjet printing. *Langmuir* **2012**, *28*, 8753–8759, PMID: 22571740.
- (25) Pauchard, L.; Allain, C. Stable and unstable surface evolution during the drying of a polymer solution drop. *Phys. Rev. E* **2003**, *68*, 052801.
- (26) Pauchard, L.; Allain, C. Mechanical instability induced by complex liquid desiccation. *Comptes Rendus Physique* **2003**, *4*, 231–239.
- (27) Pauchard, L.; Allain, C. Buckling instability induced by polymer solution drying. *EPL (Europhysics Letters)* **2003**, *62*, 897.
- (28) Wang, S.; Copeland, L. Molecular disassembly of starch granules during gelatinization and its effect on starch digestibility: a review. *Food & function* **2013**, *4*, 1564–1580.
- (29) Kim, S.; Kang, J.-H.; Song, K. B. Development of a sword bean (*Canavalia gladiata*) starch film containing goji berry extract. *Food and Bioprocess Technology* **2020**, *13*, 911–921.
- (30) Nikvarz, N.; Khayati, G. R.; Sharafi, S. Bio-based ultraviolet protective packaging film preparation using starch with incorporated date palm syrup. *Materials Chemistry and Physics* **2021**, *270*, 124794.
- (31) Yun, D.; Cai, H.; Liu, Y.; Xiao, L.; Song, J.; Liu, J. Development of active and intelligent films based on cassava starch and chinese bayberry (*Myrica rubra* Sieb. et Zucc.) anthocyanins. *RSC Adv.* **2019**, *9*, 30905–30916.

- (32) Vieira, M. G. A.; da Silva, M. A.; dos Santos, L. O.; Beppu, M. M. Natural-based plasticizers and biopolymer films: A review. *European polymer journal* **2011**, *47*, 254–263.
- (33) Jenkins, P. J.; Donald, A. M. Gelatinisation of starch: a combined SAXS/WAXS/DSC and SANS study. *Carbohydrate Research* **1998**, *308*, 133–147.
- (34) Liu, H.; Lelievre, J.; Ayoung-Chee, W. A study of starch gelatinization using differential scanning calorimetry, X-ray, and birefringence measurements. *Carbohydrate Research* **1991**, *210*, 79–87.
- (35) Zhang, B.; Dhital, S.; Flanagan, B. M.; Gidley, M. J. Mechanism for starch granule ghost formation deduced from structural and enzyme digestion properties. *Journal of Agricultural and Food Chemistry* **2014**, *62*, 760–771, PMID: 24382148.
- (36) Debet, M. R.; Gidley, M. J. Why do gelatinized starch granules not dissolve completely? Roles for amylose, protein, and lipid in granule “ghost” integrity. *Journal of Agricultural and Food Chemistry* **2007**, *55*, 4752–4760, PMID: 17503832.
- (37) Jane, J.-L.; Wong, K.-S.; McPherson, A. E. Branch-structure difference in starches of A- and B-type X-ray patterns revealed by their Naegeli dextrans. *Carbohydrate Research* **1997**, *300*, 219–227.
- (38) Cheetham, N. W.; Tao, L. Variation in crystalline type with amylose content in maize starch granules: an X-ray powder diffraction study. *Carbohydrate Polymers* **1998**, *36*, 277–284.
- (39) Domene-López, D.; García-Quesada, J.; Martín-Gullón, I.; G. Montalbán, M. Influence of starch composition and molecular weight on physicochemical properties of biodegradable films. *Polymers* **2019**, *11*, 1084.

- (40) Imberty, A.; Perez, S. A revisit to the three-dimensional structure of B-type starch. *Biopolymers* **1988**, *27*, 1205–1221.
- (41) Pichler, H.; Schmitt-Riegraf, C. *Rock-forming Minerals in Thin Section*; Springer Netherlands: Dordrecht, 1997; pp 19–27.
- (42) Okuzono, T.; Ozawa, K.; Doi, M. Simple model of skin formation caused by solvent evaporation in polymer solutions. *Physical review letters* **2006**, *97*, 136103.
- (43) Wu, Y.; Lin, Q.; Chen, Z.; Wu, W.; Xiao, H. Fractal analysis of the retrogradation of rice starch by digital image processing. *Journal of Food Engineering* **2012**, *109*, 182–187.
- (44) Utrilla-Coello, R.; Bello-Perez, L. A.; Vernon-Carter, E.; Rodriguez, E.; Alvarez-Ramirez, J. Microstructure of retrograded starch: quantification from lacunarity analysis of SEM micrographs. *Journal of Food Engineering* **2013**, *116*, 775–781.

Supporting information

Optical and structural properties of starch films formed on drying droplets of gelatinized starch solutions

Subhadip Ghosh^a, Arun Roy^a

^aRaman Research Institute, C.V. Raman Avenue, Sadashivanagar, Bangalore 560080, India.

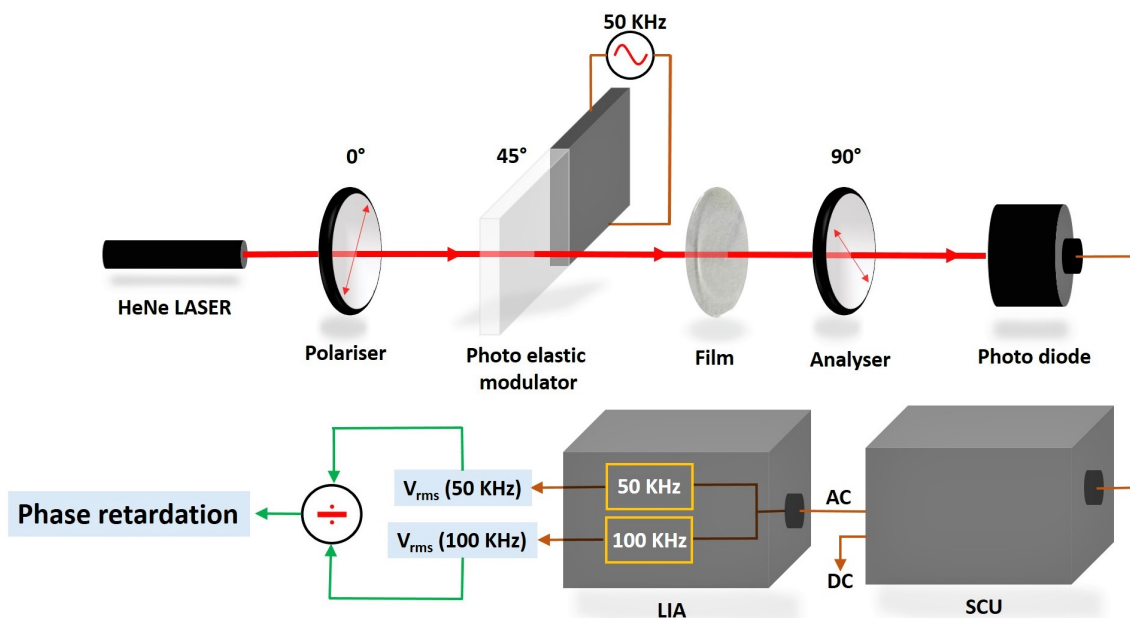


Figure S1: Schematic figure of the optical retardation measurement setup.

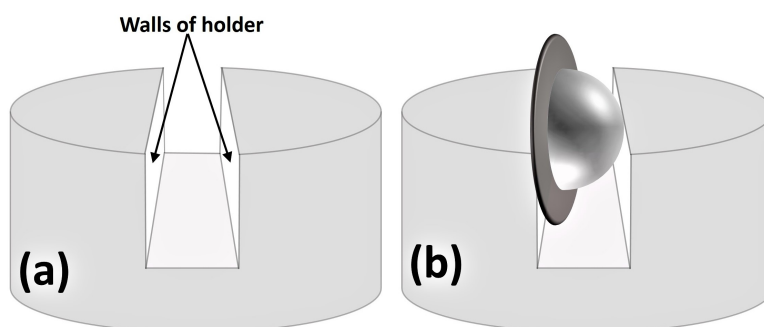


Figure S2: Schematic figures of (a) the sample holder for cryo-SEM studies and (b) the sample fixed vertically on it.

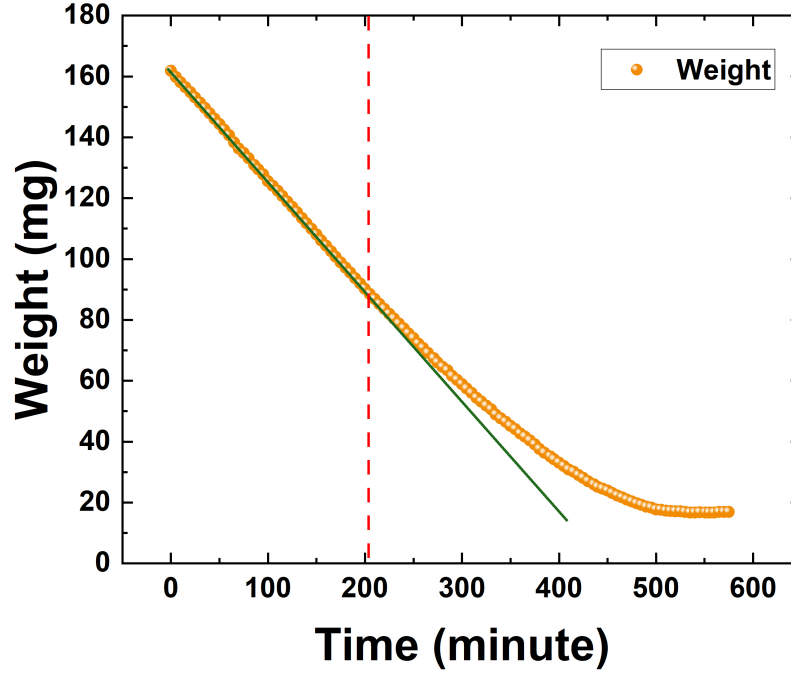


Figure S3: The variation of weight during drying of a 150 μl starch solution droplet with 9.5 wt% of initial starch concentration. The green straight line shows the initial linear variation of weight.

1 The derivation of the formula for measuring the acute axial angle

The two optic axes in the biaxial region of starch film lie on the α - γ plane where α and γ are the minor and major principal indices which are along the normal and azimuthal directions of the film respectively. The acute axial angle $2V$ between the two optic axes was calculated from the conoscopic figures. Fig. S4 shows the schematic ray diagram of the conoscopic measurement setup. The diagram depicts the light rays in the α - γ plane of the sample containing both the optic axes. In this setting, the light rays from the illuminated part of the sample kept in the front focal plane of the objective lens are focused on the rear focal plane. Hence from fig. S4, it can be written as

$$\frac{a}{f} = \tan \theta \quad (\text{S1})$$

and,

$$\frac{p}{f} = \tan V \quad (\text{S2})$$

From eqn. S1 and eqn. S2, one can write,

$$\frac{p}{a} = \frac{\tan V}{\tan \theta} = \frac{\sin V}{\cos V} \times \frac{\cos \theta}{\sin \theta} \quad (\text{S3})$$

Since the numerical aperture ($NA = n \times \sin \theta$) of the 50X objective lens used in our experiments is 0.5 and the refractive index for the intervening air medium $n = 1.0$, the value of $\theta = 30^\circ$ in our setup. Then for V between 0° and 30° , $(\cos \theta / \cos V) \approx 1$ and we can write

$$\sin V = \frac{NA \times p}{a} = \frac{NA \times 2p}{2a} \quad (\text{S4})$$

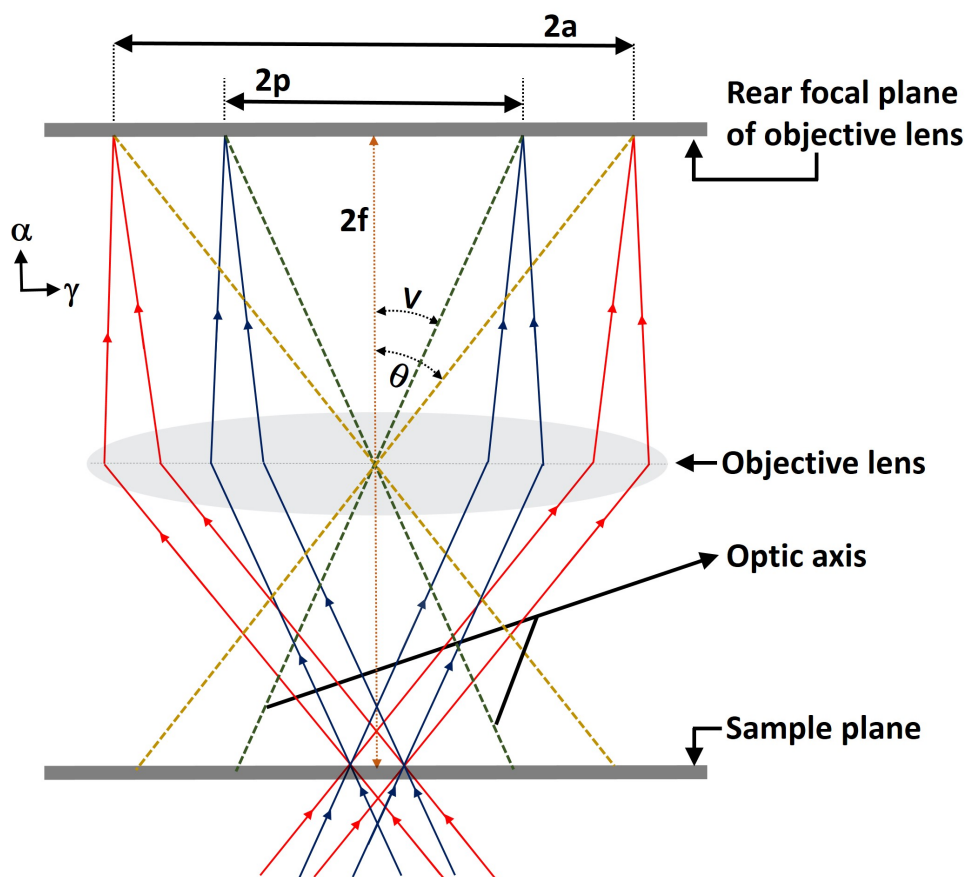


Figure S4: Schematic ray diagram of the conoscopic measurement setup.

Fig. S5 shows the schematic conoscopic figure of a biaxial region of the film when the optic plane makes an angle of 45° to the polariser. The $2p$ and $2a$ are the distance between the poles of the optic axes and the diameter of the circular field of view respectively. The acute axial angle $2V$ between the optic axes can be determined from eqn. S4 by measuring the ratio of $2p$ and $2a$.

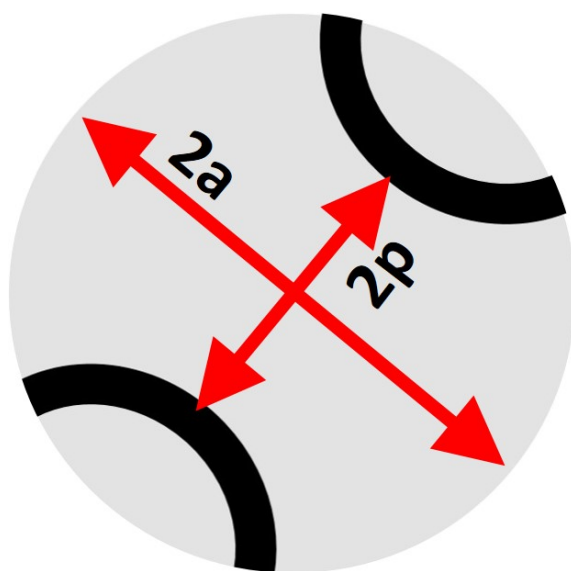


Figure S5: A schematic conoscopic figure having two uncrossed hyperbolic isogyres and also depicting the distances $2p$ and $2a$.

The conoscopic figures at different positions along the radial direction of a starch film formed from 600 μl droplet with 9.5 wt% of initial starch concentration are shown in fig. S6. The measurements were performed at an interval of 1 mm along the radial direction. The angle $2V$ between the two optic axes along the diameter of the film was calculated from these conoscopic figures by using eqn. S4.

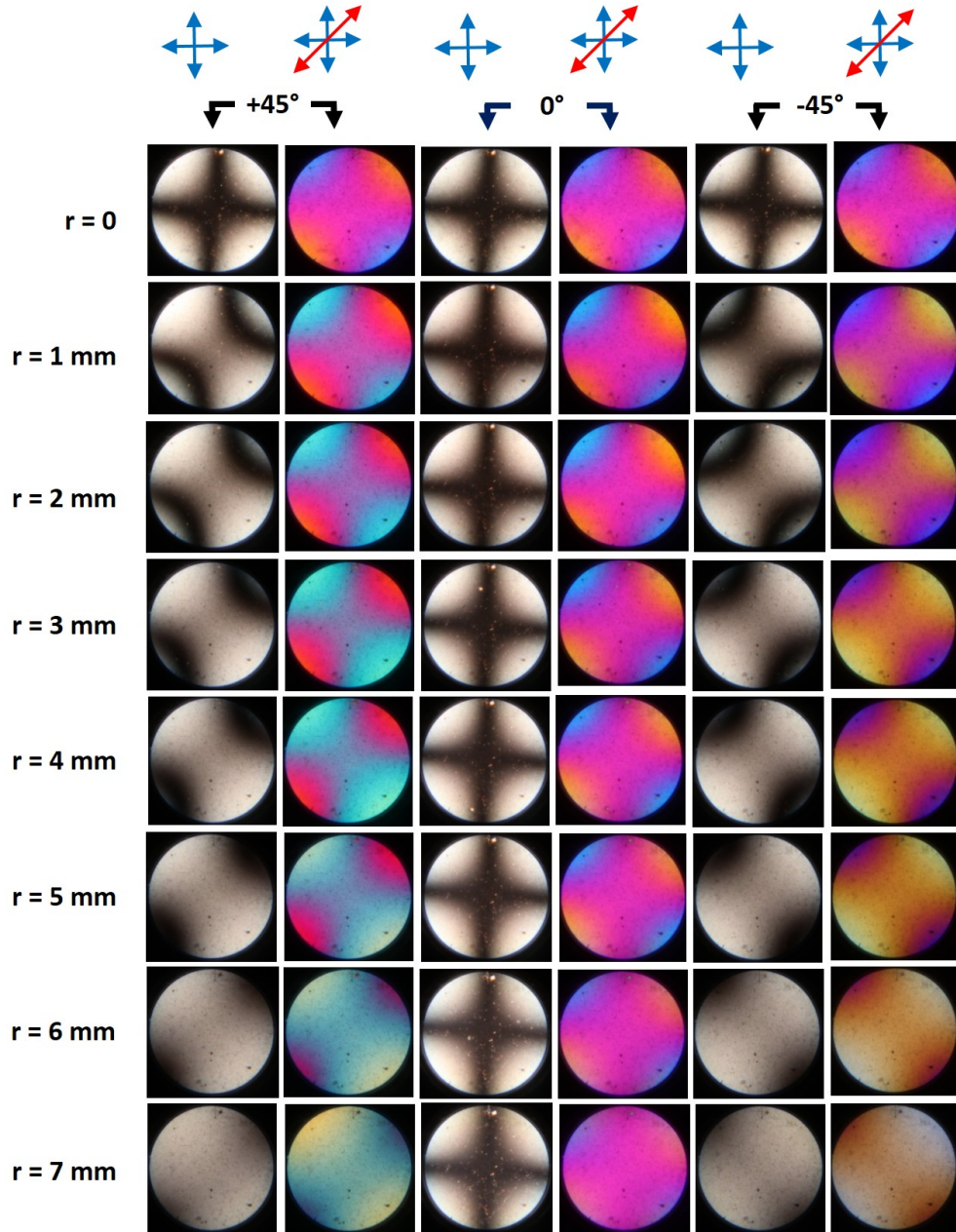


Figure S6: Conoscopic figures at different positions along the radial direction of a starch film of radius about 8 mm formed from a droplet (600 μl , 9.5 wt%). The distance between two consecutive positions of measurement is 1 mm.

2 Formula for measurement of $(\beta - \alpha)$

In the biaxial region of the circular starch film, the three principal indices α , β and γ are along the normal, radial and azimuthal directions respectively where $\alpha < \beta < \gamma$. The index ellipse in the optic

plane (i.e, α - γ plane) is shown in fig. S7. The equation of this index ellipse can be written as

$$\frac{x^2}{\gamma^2} + \frac{z^2}{\alpha^2} = 1 \quad (\text{S5})$$

where γ and α are the major and minor indices respectively. The sections of the optical indicatrix perpendicular to optic axes are circular with radius β . Therefore, the length of the radius vector to the point P on the index ellipse in fig. S7 is the intermediate index β . Then using eqn. S5, it can be shown that

$$\tan^2 V = \frac{1 - \frac{\beta^2}{\gamma^2}}{\frac{\beta^2}{\alpha^2} - 1} \quad (\text{S6})$$

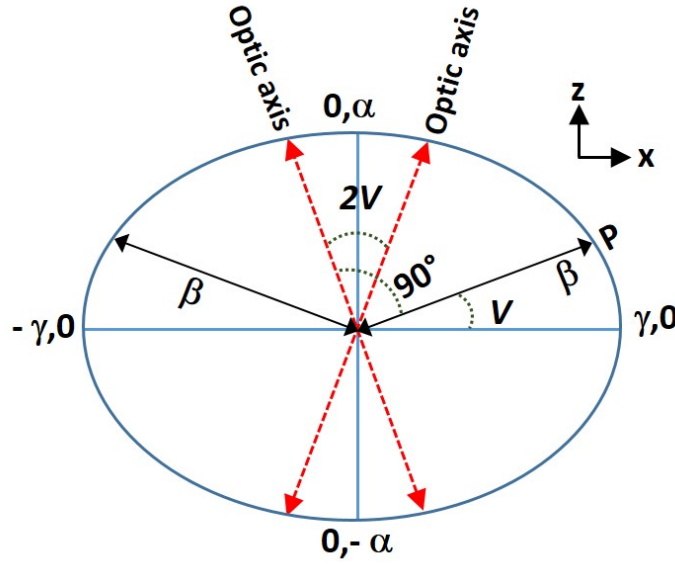


Figure S7: The index ellipse in the optic plane of starch film.

The principal refractive indices α , β and γ of starch film are expected to have similar order of magnitude to that of water or glass. The measured value of effective birefringence $(\gamma - \beta)$ of the starch films is found to be of order 10^{-4} which is very small compared to the principal values of the indices. As $60^\circ > 2V > 30^\circ$ in most of the biaxial region of the starch films (see fig. 5b in main text), it implies that $(\beta - \alpha)$ also has similar order of magnitude as that of $(\gamma - \beta)$. Therefore, using $(\gamma - \beta) \ll \beta$ and $(\beta - \alpha) \ll \beta$, eqn. S6 can be approximated as

$$\boxed{\tan^2 V = \left[\frac{\gamma - \beta}{\beta - \alpha} \right]} \quad (\text{S7})$$

or

$$\boxed{(\beta - \alpha) = \left[\frac{\gamma - \beta}{\tan^2 V} \right]} \quad (\text{S8})$$

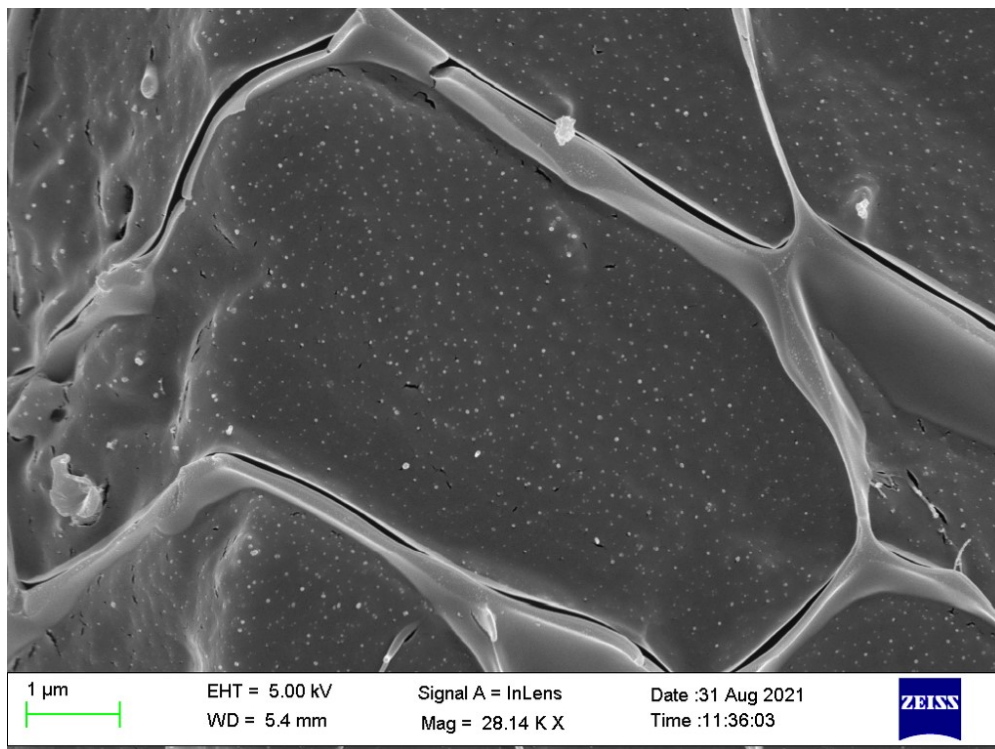


Figure S8: The cryo-SEM texture of the cross section of the starch solution droplet with 300 μl initial volume and 9.5 wt% initial starch concentration after 10 minutes of its dropcasting on a plastic substrate. The texture shows the starch nano-particles are floating in the solution bounded by the starch membranes.